J. Fluid Mech. (1995), *vol.* 304, *pp.* 27–46

Onset of stratification in a mixed layer subjected to a stabilizing buoyancy flux

By Y. NOH[1] AND H. J. S. FERNANDO[2]

[1] Department of Astronomy and Atmospheric Sciences, Yonsei University, Seoul 120-749, Korea

[2] Department of Mechanical and Aerospace Engineering, Arizona State University, Tempe, AZ 85287-6106, USA

(Received 10 June 1994 and in revised form 10 July 1995)

The formation of a thermocline in a water column, in which shear-free turbulence is generated both at the surface and bottom, and a stabilizing buoyancy flux is imposed at the surface, is studied using a laboratory experiment and a numerical model with the aim of understanding the formation of a tidal front in coastal seas. The results show that the formation of a thermocline, which always occurs in the absence of bottom mixing, is inhibited and the water column maintains a vertically mixed state, when bottom mixing becomes sufficiently strong. It is found from both experimental and numerical results that the criterion for the formation of a thermocline is determined by the balance between the rate of work that is necessary to maintain a mixed state against the formation of stratification by the buoyancy flux and the turbulent kinetic energy flux from the bottom supplied to the depth of thermocline formation. The depth of the thermocline, when it is formed, is found to decrease with bottom mixing.

1. Introduction

In coastal regions of the ocean where a relatively shallow shelf occupies large areas, the turbulence generated by the tidal friction causes the formation of a sharp boundary between the well-mixed shelf water and the stratified water of the contiguous deep ocean. To predict the position of such fronts, Simpson & Hunter (1974) proposed a criterion based on the parameter β^*, which determines whether the water column is well-mixed or stratified. The parameter β^* was obtained by considering the balance between the potential energy increase of the well-mixed state against the stratified state induced by buoyancy flux and the turbulent kinetic energy generation by the tidal friction at the bottom. This gives

$$\beta^* = HQ/U_t^3, \tag{1.1}$$

where Q is the buoyancy flux at the surface, H is the height of the water column and U_t is the amplitude of the tidal velocity. When β^* is small in shallow water ($\beta^* < 10^5$, Simpson, Allen & Morris 1978), the sea water maintains a well-mixed state with relatively uniform vertical density distribution, and the heat supplied to the surface is effectively transferred to the bottom. On the other hand, as β^* becomes larger with the increase of the water depth, a thermocline appears, which prohibits vertical heat transfer, thus making the temperature at the sea surface much higher than for the well-mixed state. The boundary between the well-mixed and stratified waters appears as a tidal front at the sea surface.

There have been numerous studies on tidal front formation (Fearnhead 1975; Simpson *et al.* 1978; Pingree & Griffiths 1978; Bye 1990). All the previous models, however, are based on the global balance between the input of kinetic energy from the

tidal friction and the demand for potential energy required to prevent stratification in the water column. A study based on microscopic considerations, in which the interaction between turbulence structure and buoyancy flux is studied to predict the variations in the vertical profiles of density with time, has not been carried out yet.

If a stabilizing buoyancy is imposed on the surface of a turbulent fluid, stratification is developed and the turbulence is suppressed; therefore the eddy diffusivity is reduced. The local reduction of the eddy diffusivity is capable of inducing even stronger stratification at a certain depth, where the turbulence is suppressed even further. This mechanism always leads to the formation of a thermocline across which both the turbulent kinetic energy flux and the buoyancy flux are prohibited, when turbulence is generated only at the surface (Noh & Fernando 1991). If turbulence is generated both at the surface and bottom, however, the kinetic energy supply from the bottom helps to keep the eddy diffusivity at a certain magnitude at the position where the thermocline is supposed to form. The turbulent kinetic energy flux from the bottom, if it becomes sufficiently strong, suppresses the feedback mechanism that leads to the formation of a thermocline; thus a well-mixed state is maintained without forming a thermocline.

Simpson & Hunter's criterion given by (1.1) applies only to the case where the bottom mixing (i.e. the turbulence generation at the bottom) by tidal friction, is predominant in comparison with the surface mixing (i.e. the turbulence generation at the sea surface) by wind shear. Nevertheless the importance of surface mixing is evident from its critical role in the formation of a thermocline as mentioned above, although its effects are often obscured by the fact that the wind field does not vary significantly over the large area of the sea surface (Simpson *et al.* 1978). The contribution of wind stress has often been included in previous models (for example, Simpson *et al.* 1978; Fearnhead 1975), but its effects on the formation of a thermocline have not been studied rigorously.

To investigate the mechanism for tidal front formation a laboratory experiment was carried out by Hopfinger & Linden (1982). A stabilizing buoyancy flux (by heat) was imposed on the water surface and shear-free turbulence was generated by an oscillating grid located near the bottom. They observed that the surface temperature increases much faster than that expected from uniform mixing over the whole water column if the criterion

$$\beta_0 = H^4 Q / K_{0b}^3 > A_1 \tag{1.2}$$

is satisfied, where K_{0b} is the eddy diffusivity at the bottom and A_1 is a constant. The parameter β_0 can be modified to

$$\beta_{0H} = HQ/u_H^3 > A_2, \tag{1.3}$$

since the local r.m.s. turbulent velocity u is given by $u \sim K_{0b}/z$ for the turbulence generated by the grid oscillation, where z is the vertical distance from the grid near the bottom, $u_H = u(z = H)$ and A_2 is a constant. Assuming that u_H is proportional to U_t, Hopfinger & Linden (1982) argued that (1.3) is equivalent to (1.1) with $u_H/U_t \approx 2 \times 10^{-2}$ based on a comparison between the experimental data and Simpson & Hunter's criterion. However, note that u_H decreases with H while U_t is independent of it. Moreover, a realistic two-layer system with a thermocline at a certain depth, could not be produced. Instead a runaway temperature stratification developed within a very thin surface layer, because turbulence was not generated at the surface and the turbulence level near the surface was suppressed severely owing to the imposed stabilizing buoyancy flux. This clearly points to the importance of surface mixing.

In this paper, the formation of a thermocline in a turbulent layer subjected to a

surface stabilizing buoyancy flux is investigated for the case where the shear-free turbulence is generated both at the surface and at the bottom. A laboratory experiment and a numerical model are used for this purpose. In the laboratory experiment shear-free turbulence is generated from two oscillating grids, one located near the surface and the other near the bottom of a water column, and stabilizing buoyancy flux is imposed on the surface. For the numerical model, a one-dimensional turbulence model is developed based on the model by Noh (1993), in which the interaction between turbulence structure and density stratification is taken into account to elucidate the formation of a thermocline in shear-free turbulence. In both cases the evolution of vertical density profiles is studied. Results are compared with each other and are used to examine the emergence of a thermocline for given conditions. A criterion for the formation of a thermocline is suggested and, when a thermocline does form, its depth is obtained. The results are also discussed in the light of the previous studies.

2. Experiments

2.1. *The apparatus*

A schematic diagram of the experimental apparatus is shown in figure 1. The test cell was a Plexiglas tank of cross-section 25.4 cm × 25.4 cm and height 45.7 cm. In all experiments the height of the water column was fixed at 36.5 cm. The centres of the oscillating grids were located 3 cm below the water surface and the 8 cm above the bottom, respectively. Thus the distance between the two grids was 25.5 cm. The grids were made of 0.95 cm square Plexiglas bars with mesh size $M = 4.75$ cm. The strokes, S_s and S_b, and the frequencies, f_s and f_b, of the grid oscillations near the surface and the bottom, respectively, could be varied in the ranges $0.8 < S_s, S_b < 2.0$ cm and $1 < f_s, f_b < 5$ Hz.

The stabilizing buoyancy flux was produced by adding fresh water continuously to the top of the fluid column which initially consisted of uniform saline water. The fresh water was introduced to the surface through a vertical glass tube of diameter 0.8 cm, which was connected to an overhead reservoir. The fresh water from the tube was released onto a sparsely perforated Plexiglas plate which was placed horizontally 5 cm above the water surface; in this way a uniform distribution of fresh water over the water surface was possible. Strong grid-oscillation-generated turbulence near the surface produced rapid mixing of incoming fresh water with the saline water in the tank. The mixed fluid was allowed to overflow through four holes located on each side of the tank, thus keeping the height of the water column constant during the experiment. The surface buoyancy flux Q could be determined by $Q = g\Delta\rho V/\rho$, where V is the volume flux per unit area at which the fresh water is supplied to the surface, $\Delta\rho/\rho$ is the fractional density difference between the incoming fresh water and the saline water in the mixed layer, and g is the gravitational acceleration. The influx rate of fresh water was adjusted at two-minute intervals using a flow meter and a valve attached to the overhead reservoir according to the density of the mixed layer at the moment so as to maintain a constant buoyancy flux throughout the experiment. The density of the upper mixed layer was continuously monitored on the voltmeter connected to the conductivity probe.

2.2. *The experimental procedure*

First, both grids were set to oscillate at predetermined frequencies. Once the turbulence was fully established after a few minutes, the buoyancy flux was switched on at time $t = 0$. Density profiles were measured every 2 min using a conductivity probe and a

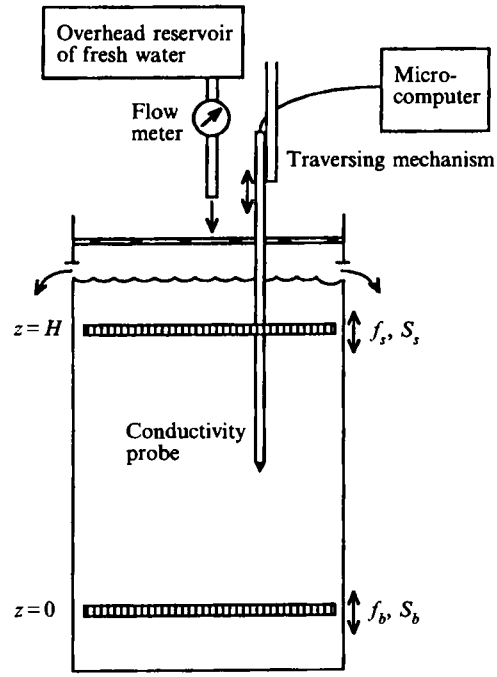

FIGURE 1. A schematic view of the experimental setup.

potentiometer, which were mounted on a stepping-motor-driven transversing mechanism. Typically an experiment lasted between 30 min and 2 h depending on the buoyancy flux.

In some experiments, the laser-induced fluorescence (LIF) method was employed to visualize mixing processes. Ethyl alcohol was added to the fresh water in the overhead tank so that the refractive indices of the incoming fresh water were matched with the saline water in the tank. Then a small amount of Rhodamine 6G was added to the fresh water for visualization. Fluorescent light was emitted from Rhodamine 6G when a sheet of argon–ion laser light illuminated it, and it was photographed by a camera through a filter which allows only the emitted fluorescent light to pass. The light intensity, proportional to the concentration of Rhodamine 6G, was used to represent the concentration of the fresh water introduced in the fluid.

2.3. *The characteristics of the turbulence generated by the grid oscillation*

The characteristics of shear-free turbulence generated by grid oscillation in homogeneous fluids have been studied extensively (Hopfinger & Toly 1976; Hannoun, Fernando & List 1988; Noh & Fernando 1993). These studies showed that the horizontal and vertical r.m.s. velocities (u_s, w_s) and the integral length scale l_s of the turbulence can be expressed as

$$l_s = a_1(H-z+z_0), \tag{2.1}$$

$$u_s = a_2 S_s^{3/2} M^{1/2} f_s (H-z+z_0)^{-1}, \tag{2.2}$$

and

$$w_s = a_3 u_s, \tag{2.3}$$

when the grid is located near the surface. Here constants a_1, a_2 and a_3 and the virtual origin z_0 are dependent on the grid geometry. Noh & Fernando (1993) estimated $a_1 = 0.1$, $a_2 = 0.13$ and $a_3 = 1.3$ for the configuration used in the present experiment using single-component laser–Doppler velocimeter (LDV) measurements.

Similarly, the horizontal and vertical r.m.s. velocities (u_b, w_b) and the integral length scale l_b of turbulence generated by the grid oscillation near the bottom are

$$l_b = a_1(z+z_0), \tag{2.4}$$

$$u_b = a_2 S_b^{3/2} M^{1/2} f_b (z+z_0)^{-1}, \tag{2.5}$$

and

$$w_b = a_3 u_b. \tag{2.6}$$

Note that in order to be consistent with its physical meaning in (1.1) the height of a water column H is defined by the distance between the centres of the grids near the surface and the bottom rather than the actual height of the water column.

3. Formulation of the mathematical model

The two turbulent fields induced by two independent grid oscillations are assumed to be uncorrelated each other, so that the turbulent kinetic energy E can be represented by the superposition of the two turbulent kinetic energies E_s and E_b generated when only one grid is oscillated either at the surface (E_s) or at the bottom (E_b) while the other one remains stationary. That is

$$E = E_s + E_b. \tag{3.1}$$

The above assumption (3.1) has been recently confirmed for the case of homogeneous fluids by Srdic, Fernando & Montenegro (1995) in experiments with two oscillating grids similar to those in figure 1. This assumption is also observed to be valid when a density interface is present as was demonstrated by Turner (1986). Taking both these experimental results into consideration, it is possible to expect that the turbulent kinetic energy can be always represented by (3.1), whether a density interface is formed or not.

In accordance with this it can be further assumed that the mean buoyancy B is diffused by both turbulent fields simultaneously so that

$$\frac{\partial B}{\partial t} = \frac{\partial}{\partial z}\left[(K_s + K_b)\frac{\partial B}{\partial z}\right], \tag{3.2}$$

where K_s and K_b are the respective eddy diffusivity corresponding to E_s and E_b.

The equations for E_s and E_b can be expressed as

$$\frac{\partial E_s}{\partial t} = \frac{\partial}{\partial z}\left(K_s \frac{\partial E_s}{\partial z}\right) + K_s \frac{\partial B}{\partial z} - \epsilon_s, \tag{3.3}$$

$$\frac{\partial E_b}{\partial t} = \frac{\partial}{\partial z}\left(K_b \frac{\partial E_b}{\partial z}\right) + K_b \frac{\partial B}{\partial z} - \epsilon_b. \tag{3.4}$$

The terms on the right-hand sides of (3.3) and (3.4) represent respectively the turbulent kinetic energy flux, the buoyancy flux and the dissipation rate of turbulent kinetic energy (Noh & Fernando 1991). The eddy diffusivities K_s and K_b and the dissipation rates ϵ_s and ϵ_b can be modelled as

$$K_s = c_\mu E_s^{1/2} l_s, \tag{3.5}$$

$$K_b = c_\mu E_b^{1/2} l_b, \tag{3.6}$$

$$\epsilon_s = c_D E_s^{3/2} l_s^{-1}, \tag{3.7}$$

$$\epsilon_b = c_D E_b^{3/2} l_b^{-1}, \tag{3.8}$$

if it is assumed that the turbulent fields generated at the surface and bottom have their own respective inertial scales l_s and l_b, where c_μ and c_D are constants.

Information on the velocity and length scales of turbulence, required to calculate (3.5)–(3.8), can be obtained from experimental data such as (2.1)–(2.6), although note that (2.1)–(2.6) are valid only for homogeneous fluids. Experimental and theoretical studies (Britter *et al.* 1983; Pearson, Puttock & Hunt 1983; Csanady 1964) have shown that, in stably stratified fluids, the growth of the vertical length scale of turbulence l_{sv} is limited by the buoyancy length scale $l_{sN}(=u_s/N$, where N is the Brunt–Väisälä frequency). On this basis it is assumed that l_{sv} has the form

$$l_{sv} = \frac{l_{sn}}{[1+(l_{sn}/c_l l_{sN})^2]^{1/2}}, \tag{3.9}$$

where l_{sn} is the length scale of turbulence in a homogeneous fluid given by (2.1) and c_l is a constant of order one (Andre *et al.* 1978; Galperin *et al.* 1989). If the length scale is rescaled as $l'_{sv} = l_{sv}/a_1$, (3.5) and (3.7) can be written as

$$K_s = c'_\mu E_s^{1/2} l'_{sv}, \tag{3.10}$$

$$\epsilon_s = c'_D E_s^{3/2} l'^{-1}_{sv}, \tag{3.11}$$

where $c'_\mu = a_1 c_\mu$ and $c'_D = c_D/a_1$.

Similarly (3.6) and (3.8) become

$$K_b = c'_\mu E_b^{1/2} l'_{bv}, \tag{3.12}$$

$$\epsilon_b = c'_D E_b^{3/2} l'^{-1}_{bv}, \tag{3.13}$$

and the vertical length scale of turbulence under the influence of stratification is given by

$$l_{bv} = \frac{l_{bn}}{[1+(l_{bn}/c_l l_{bN})^2]^{1/2}}, \tag{3.14}$$

where l_{bn} is the length scale of turbulence in a homogeneous fluid given by (2.4) and $l_{bN} = u_b/N$.

Again by rescaling of t by $t' = c'_\mu t$, (3.2), (3.3) and (3.4) can be rewritten as

$$\frac{\partial E_s}{\partial t'} = \frac{\partial}{\partial z}\left(K'_s \frac{\partial E_s}{\partial z}\right) + K'_s \frac{\partial B}{\partial z} - \left(\frac{c'_D}{c'_\mu}\right)\epsilon'_s, \tag{3.15}$$

$$\frac{\partial E_b}{\partial t'} = \frac{\partial}{\partial z}\left(K'_b \frac{\partial E_b}{\partial z}\right) + K'_b \frac{\partial B}{\partial z} - \left(\frac{c'_D}{c'_\mu}\right)\epsilon'_b, \tag{3.16}$$

$$\frac{\partial B}{\partial t'} = \frac{\partial}{\partial z}\left[(K'_s + K'_b)\frac{\partial B}{\partial z}\right], \tag{3.17}$$

where

$$K'_s = E_s^{1/2} l'_{sv}, \tag{3.18}$$

$$\epsilon'_s = E_s^{3/2} l'^{-1}_{sv}, \tag{3.19}$$

$$K'_b = E_b^{1/2} l'_{bv}, \tag{3.20}$$

$$\epsilon'_b = E_b^{3/2} l'^{-1}_{bv}. \tag{3.21}$$

For (3.15) and (3.16), $c'_D/c'_\mu = 6$ can be obtained by substituting the characteristic velocity and length scales of turbulence generated by grid oscillation such as (2.1)–(2.3) into the steady-state form of (3.15) (or (3.16)) in a homogeneous fluid with $\partial B/\partial z = 0$

(Noh & Fernando 1991). It is important to note that no empirical constants appear in (3.15)–(3.21), once $c'_D/c'_\mu = 6$ is determined.

By defining $U = [E_s(H, t')]^{1/2}$ and $L = l'_s(H, t')$, it is possible to define the non-dimensional variables as

$$\left.\begin{gathered} E_s^* = \frac{E_s}{U^2}, \quad l_{sv}'^* = \frac{l'_{sv}}{L}, \quad E_b^* = \frac{E_b}{U^2}, \quad l_{bv}'^* = \frac{l'_{bv}}{L}, \\ K_s'^* = \frac{K'_s}{(UL)}, \quad \epsilon_s'^* = \frac{\epsilon'_s}{(U^3/L)}, \quad K_b'^* = \frac{K'_b}{(UL)}, \quad \epsilon_b'^* = \frac{\epsilon'_b}{(U^3/L)}, \\ z^* = \frac{z}{L}, \quad t'^* = \frac{t'}{(L/U)}, \quad H^* = \frac{H}{L}. \end{gathered}\right\} \tag{3.22}$$

The non-dimensionalization of B is

$$B^* = \frac{B}{Q/(c'_\mu U)}. \tag{3.23}$$

In what follows in this Section, the asterisks on the non-dimensional variables will be dropped. The non-dimensional forms of (3.15)–(3.17) are now given as

$$\frac{\partial E_s}{\partial t'} = \frac{\partial}{\partial z}\left(K'_s \frac{\partial E_s}{\partial z}\right) + GK'_s \frac{\partial B}{\partial z} - 6\epsilon'_s, \tag{3.24}$$

$$\frac{\partial E_b}{\partial t'} = \frac{\partial}{\partial z}\left(K'_b \frac{\partial E_b}{\partial z}\right) + GK'_b \frac{\partial B}{\partial z} - 6\epsilon'_b, \tag{3.25}$$

$$\frac{\partial B}{\partial t'} = \frac{\partial}{\partial z}\left[(K'_s + K'_b)\frac{\partial B}{\partial z}\right], \tag{3.26}$$

where
$$G = Q/(U^3/L), \tag{3.27}$$

and
$$K'_s = E_s^{1/2} l'_{sv}, \tag{3.28}$$

$$\epsilon'_s = E_s^{3/2} l_{sv}'^{-1}, \tag{3.29}$$

$$K'_b = E_b^{1/2} l'_{bv}, \tag{3.30}$$

$$\epsilon'_b = E_b^{3/2} l_{bv}'^{-1}. \tag{3.31}$$

Further, the modification of the vertical length scale by the stratification, which is given by (3.9) and (3.14), can be rewritten as

$$l'_{sv} = l'_{sn}/(1 + c_R Ri_s)^{1/2}, \tag{3.32}$$

where
$$Ri_s = 3l_{sn}'^2 N^2/2E_s, \tag{3.33}$$

$$= -\frac{3l_{sn}'^2}{2E_s} G \frac{\partial B}{\partial z}, \tag{3.34}$$

and
$$l'_{bv} = l'_{bn}/(1 + c_R Ri_b)^{1/2}, \tag{3.35}$$

where
$$Ri_b = 3l_{bn}'^2 N^2/2E_b, \tag{3.36}$$

$$= -\frac{3l_{bn}'^2}{2E_b} G \frac{\partial B}{\partial z} \tag{3.37}$$

and
$$c_R = (a_1/c_l)^2. \tag{3.38}$$

The initial conditions are taken to be

$$E_s(z,0) = (1+H-z)^{-2}, \tag{3.39}$$

$$E_b(z,0) = (1+z)^{-2}, \tag{3.40}$$

$$B(z,0) = 0, \tag{3.41}$$

which represent the superposition of the turbulent fields generated by the grid oscillations at the surface and at the bottom in the absence of buoyancy flux. It is assumed that the buoyancy flux is suddenly imposed on the surface at $t' = 0$. The boundary conditions are then given by

$$E_s(H,t') = 1, \tag{3.42}$$

$$\frac{\partial E_s(0,t')}{\partial z} = 0, \tag{3.43}$$

$$\frac{\partial E_b(H,t')}{\partial z} = 0, \tag{3.44}$$

$$E_b(0,t') = \alpha, \tag{3.45}$$

$$\frac{\partial B(H,t')}{\partial z} = -[1+K_b'(H,t')]^{-1}, \tag{3.46}$$

$$\frac{\partial B(0,t')}{\partial z} = 0, \tag{3.47}$$

where $\alpha(\equiv U_b^2/U_s^2)$ is the ratio of turbulent kinetic energy at the bottom ($U_b^2 \equiv E_b(z=0)$) to that at the surface ($U_s^2 \equiv E_s(z=H)$). The parameter c_R which represents the effect of stratification on the vertical length scale has been estimated to be $c_R = 0.1$ by Noh & Fernando (1991) from a comparison of the numerical results of the depth of a thermocline with the experimental data. The calculations were performed using an implicit finite-difference method. The height of the water column was fixed at $H = 100$.

4. Dimensional analysis

When there is turbulence generation by grid oscillation only at the surface while the stabilizing buoyancy flux is imposed on it, the formation of a thermocline is found to be determined by the eddy diffusivity at the surface K_{0s} and the buoyancy flux at the surface Q (Kantha & Long 1980; Hopfinger & Linden 1982; Noh & Long 1990; Noh & Fernando 1991). This leads to the prediction of the depth of the thermocline D_0 as

$$D_0 \propto (K_{0s}^3/Q)^{1/4}. \tag{4.1}$$

In the presence of turbulence generation at the bottom two more parameters will be relevant to the phenomena, namely the eddy diffusivity at the bottom K_{0b} and the height of water column H, in addition to K_{0s} and Q. That is, the criterion for the formation of a thermocline is determined by

$$f(H, K_{0b}, K_{0s}, Q) = 0. \tag{4.2}$$

Here the eddy diffusivities K_{0b} and K_{0s} in (4.2) can be replaced by K_{0b}' and K_{0s}', which are the variables used in the numerical model, since they differ only in a proportional constant (i.e. $K_{0b} = c_\mu' K_{0b}'$). That is

$$f(H, K_{0b}', K_{0s}', Q) = 0. \tag{4.3}$$

The use of K'_{0b} and K'_{0s} is also advantageous for the comparison with the experimental data, because they can be evaluated directly from the experimental conditions of (2.1)–(2.6) without using empirical constants such as c_μ and a_1.

The parameters in (4.3) are then non-dimensionalized by K'_{0b} and H to give

$$f\left(\frac{Q}{K'^3_{0b}/H^4}, \frac{K'_{0s}}{K'_{0b}}\right) = 0. \tag{4.4}$$

Since the length scale of turbulence generated by grid oscillation is constant regardless of the frequency and the position of grid oscillation (Hopfinger & Toly 1976; Hannoun *et al.* 1988), relation (4.4) can be rewritten as

$$f\left(\left(\frac{H}{L}\right)^3 \frac{HQ}{U_b^3}, \frac{U_s}{U_b}\right) = 0 \tag{4.5}$$

or

$$f(\alpha, \beta) = 0, \tag{4.6}$$

where $\beta \equiv H^4Q/K'^3_{0b} (= (H/L)^3 HQ/U_b^3)$ and $\alpha = U_b^2/U_s^2$. Note that in the absence of surface mixing (i.e. $\alpha = \infty$), (4.5) reduces to the criterion (1.2) given by Hopfinger & Linden (1982). On the other hand, the same criterion can be expressed by non-dimensionalization in terms of K'_{0s} and H as

$$f(\alpha, \gamma) = 0, \tag{4.7}$$

where $\gamma \equiv H^4Q/K'^3_{0s} = (H/L)^4 G = \beta\alpha^{3/2}$.

Further, the depth of a thermocline at which the density jump occurs, D, can be expressed as

$$D = f(H, K'_{0s}, K'_{0b}, Q), \tag{4.8}$$

and using non-dimensionalization in terms of K'_{0s} and Q it is possible to obtain

$$\frac{D}{(K'^3_{0s}/Q)^{1/4}} = f\left(\frac{K'_{0b}}{K'_{0s}}, \frac{H}{(K'^3_{0s}/Q)^{1/4}}\right), \tag{4.9}$$

or

$$D/D_0 = f(\alpha, \gamma), \tag{4.10}$$

where D_0 is given by

$$D_0 = A_3(K'^3_{0s}/Q)^{1/4} \tag{4.11}$$

or

$$D_0/H = A_3\gamma^{-1/4} \tag{4.12}$$

with $A_3 \approx 6.6$ (Noh & Fernando 1991). Note that when there is no bottom mixing ($\alpha = 0$), the dependence on γ in (4.10) disappears, too.

5. Results

5.1. *Experimental results*

It is observed in the experiments with no bottom mixing that a thermocline always develops as in previous experiments as long as H is larger than D_0 (Kantha & Long 1980; Hopfinger & Linden 1982; Noh & Long 1990). When the intensity of bottom mixing becomes sufficiently large, however, the mixed layer is maintained throughout the entire water column without forming a thermocline.

The photographs in figure 2(*a–c*), obtained using the LIF method, show the variation of mixing patterns with the increase of the bottom mixing when the buoyancy flux and the surface mixing are held fixed ($\gamma = 879$). In the absence of bottom mixing

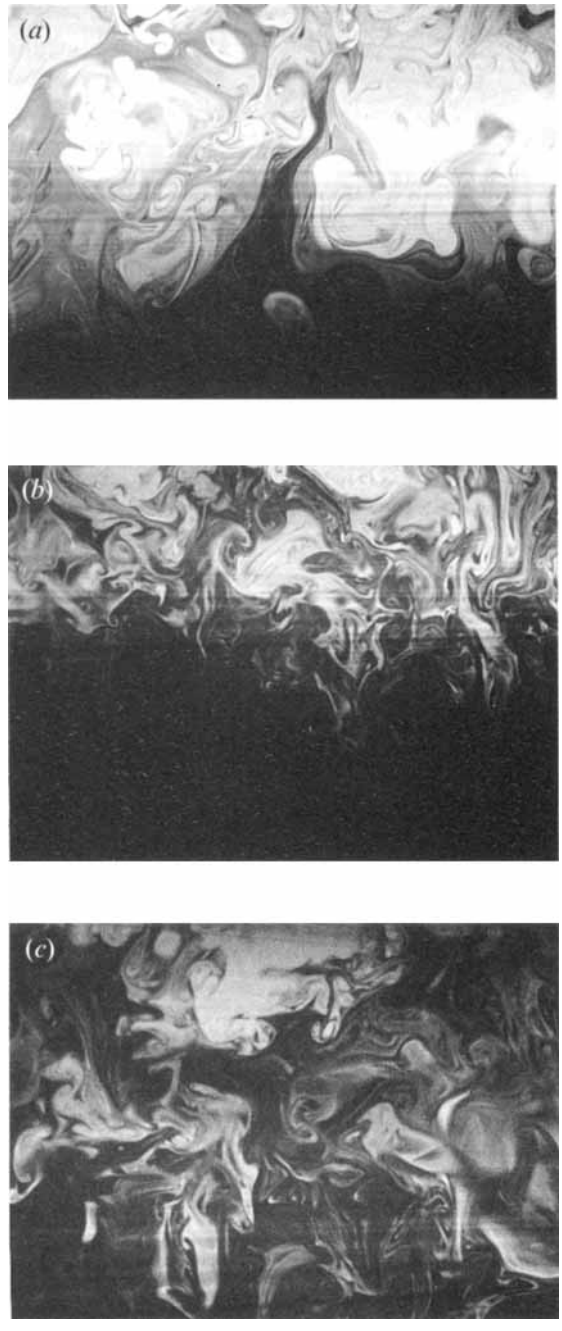

FIGURE 2. The variations of the patterns of turbulence mixing with the increase of the bottom mixing at $\gamma = 879$ when $t = 5$ min. The incoming fresh water is dyed with Rhodamine 6G, and the top and the bottom of each photograph corresponds to $z = 8$ cm and $z = 20$ cm, respectively: (*a*) $\alpha = 0$, (*b*) $\alpha = 5.72$, (*c*) $\alpha = 11.39$.

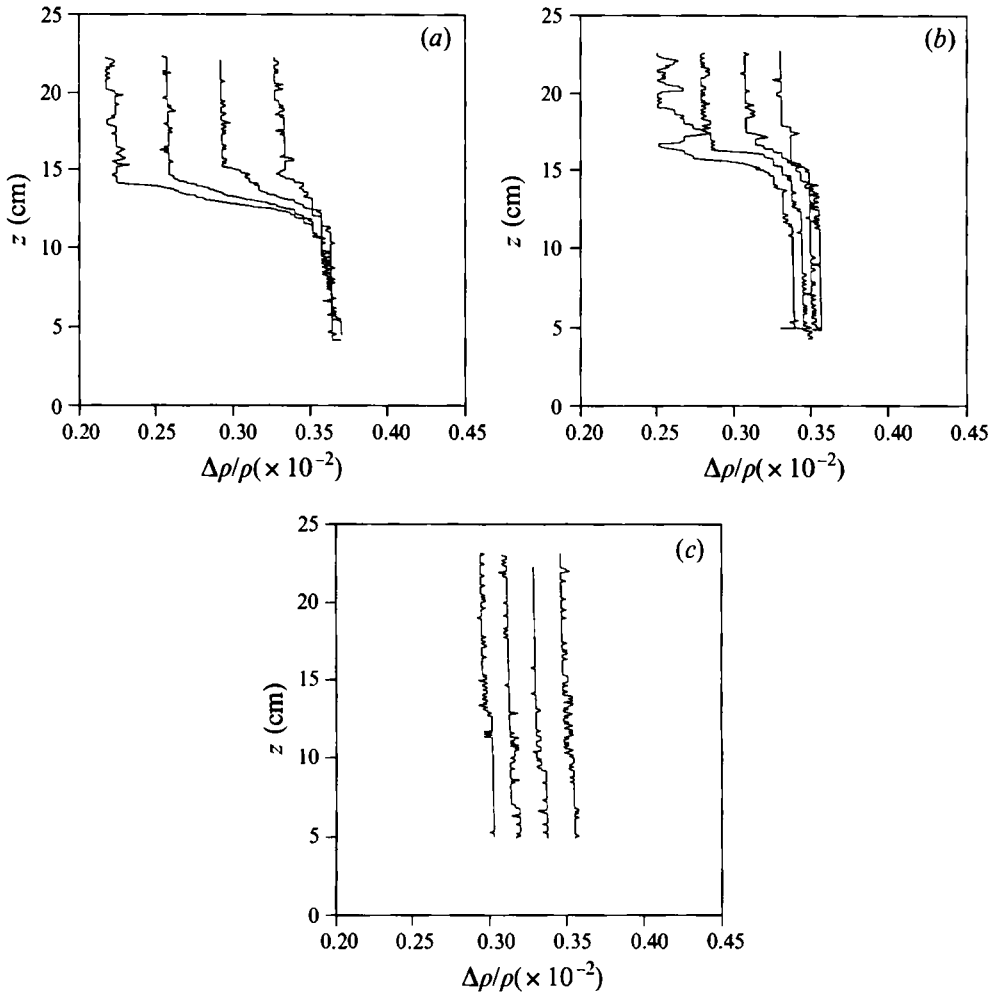

FIGURE 3. The evolution of the vertical density profiles obtained from the laboratory experiments with time when $\gamma = 879$. Each graph corresponds to $t = n\Delta t (n = 1 \ldots 4, \Delta t = 10$ min): (*a*) $\alpha = 0$, (*b*) $\alpha = 5.72$, (*c*) $\alpha = 11.39$.

($\alpha = 0$, figure 2*a*), the fluid motion near the thermocline is weak and devoid of small-scale activity. A thermocline is formed where the downward motion of turbulence is bounded by the buoyancy force due to stabilizing buoyancy flux. When there is bottom mixing ($\alpha = 5.72$, figure 2*b*), the thermocline is disturbed by the turbulence propagating upward from the bottom, and relatively strong turbulent kinetic energy exists there. When the bottom mixing is strong ($\alpha = 11.39$, figure 2*c*), vigorous turbulent mixing can be maintained over the entire water column, and the thermocline does not develop. The time required for the appearance of a thermocline increases with the decrease of Q and with the increase of K_{0s} and K_{0b} as predicted by Noh & Fernando (1991), but it is less than 5 min, in most of the experiments, before a thermocline is formed.

Similar inferences can be made using the vertical density profiles measured by a conductivity probe ($\gamma = 879$, figure 3*a–c*). Figure 3(*a*) shows that a thermocline develops with time in the absence of bottom mixing ($\alpha = 0$). In this case the density in the lower layer remains unaffected by the surface buoyancy flux. When a thermocline

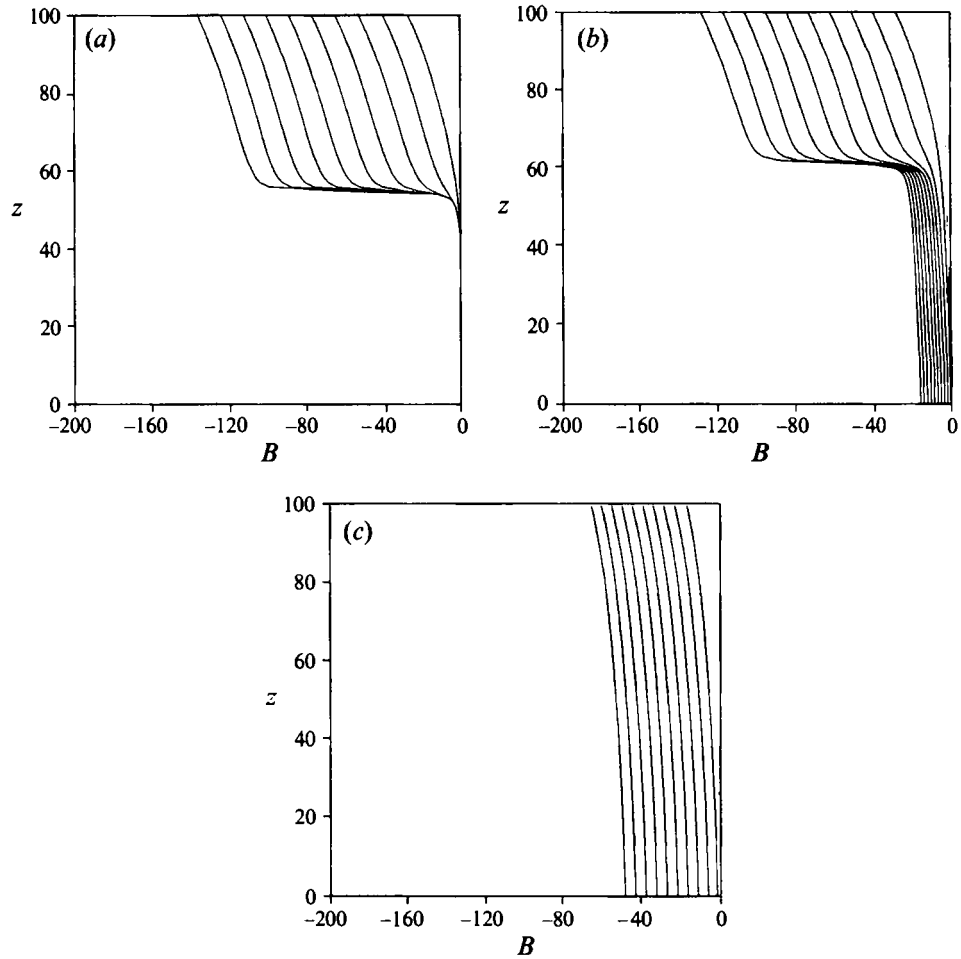

FIGURE 4. The evolution of the vertical density profiles obtained from the numerical model with time when $\gamma = 800$. Each graph corresponds to $t' = n\Delta t'(n = 1 \ldots 10, \Delta t' = 400)$: (*a*) $\alpha = 0$, (*b*) $\alpha = 2.0$, (*c*) $\alpha = 16.0$.

is formed in the presence of weak bottom mixing ($\alpha = 5.72$, figure 3*b*), the density jump appears soon after the start of the buoyancy flux, and the density difference between the surface and the bottom increases with time. In this case the density in the lower layer, however, decreases slowly with time, suggesting the existence of vertical buoyancy transfer across the thermocline. Often, large-scale fluctuations of the density profile are observed (for example, $t = 40$ min in figure 3*b*), suggesting the existence of strong mixing by large eddies across the thermocline. When a thermocline is not formed owing to the strong bottom mixing ($\alpha = 11.39$, figure 3*c*), the density of the water column decreases with time rather uniformly, maintaining the density difference between the surface and the bottom invariant with time. It is also observed that the rate of density decrease at the surface ($z = H$) with time is much slower than for cases where a thermocline is formed, because the buoyancy flux is transferred over the entire depth of the water column in this case. For the well-mixed state, experiments were usually run for more than 3 h to ensure that there is no formation of a thermocline. A detailed discussion on the determination of the state of a water column will be given in §5.3.

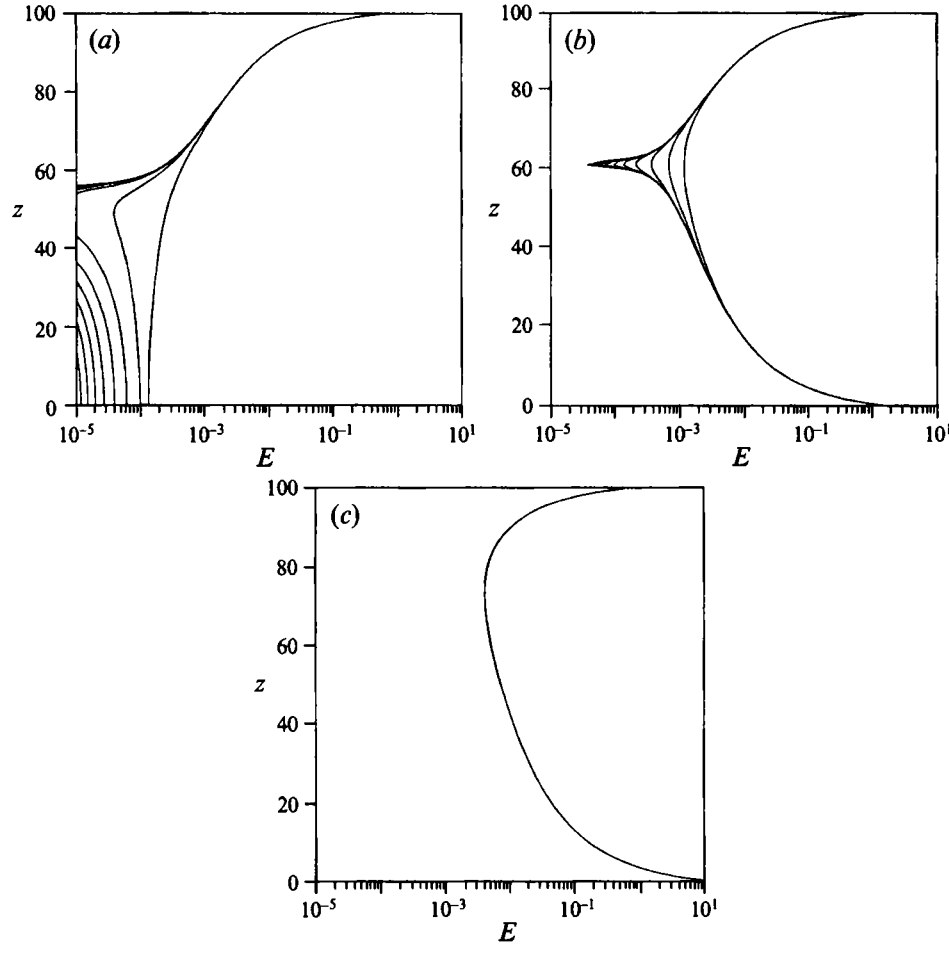

FIGURE 5. The evolution of the turbulent kinetic energy from the numerical model with time when $\gamma = 800$. Each graph corresponds to $t' = n\Delta t'(n = 1 \ldots 10, \Delta t' = 400)$: (*a*) $\alpha = 0$, (*b*) $\alpha = 2.0$, (*c*) $\alpha = 16.0$.

5.2. *Numerical results*

The corresponding results of the time evolution of the vertical density distribution $B(z, t')$ from the numerical model are shown in figure 4(*a–c*) with increasing values of α for a given $\gamma(= 800)$. They show the formation of a thermocline with and without bottom mixing (figure 4*a*, *b*) and no formation of a thermocline under strong bottom mixing (figure 4*c*), respectively.

Figure 5(*a–c*) shows the evolution of turbulent kinetic energy $E(= E_b + E_s)$ with time for each case of figure 4(*a–c*). When a thermocline does not develop, the turbulent kinetic energy remains unchanged from the initial state. However, when a thermocline does develop, the turbulent kinetic energy decreases sharply with time at the depth of the thermocline, which results in reduced eddy diffusivity there.

5.3. *A criterion for the formation of a thermocline*

It was noted in the previous section that the density difference between the surface and the bottom increases linearly with time for the case of thermocline formation, because buoyancy flux is prohibited across the thermocline; on the other hand for the well-

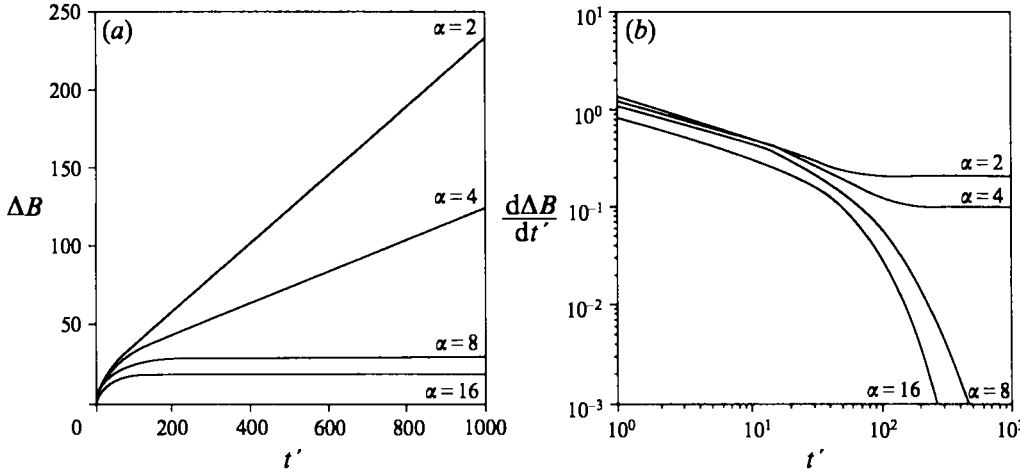

FIGURE 6. (*a*) The variation of the density difference between the surface and the bottom $\Delta B(\equiv B(0,t')-B(H,t'))$, and (*b*) the variation of $\mathrm{d}\Delta B/\mathrm{d}t'$ with time for various values of α when $\gamma = 800$.

mixed state it becomes constant after some time. Figure 6(*a*) shows the variations of the density difference between the surface and the bottom $\Delta B(\equiv B(0,t')-B(H,t'))$ with time for different values of α when $\gamma = 800$. It is found that ΔB increases linearly with time when a thermocline is formed ($\alpha \leqslant 4.0$), while it converges to a certain value when the thermocline is not formed ($\alpha \geqslant 8.0$). The difference between two cases is revealed more clearly in the variation of $\mathrm{d}\Delta B/\mathrm{d}t'$ with time (figure 6*b*); it remains at a certain value after some time for $\alpha \leqslant 4.0$, while it decreases continuously with time for $\alpha \geqslant 8.0$. From this it is possible to discern the case of thermocline formation ('the stratified state') from that of no formation ('the well-mixed state').

The same criterion was applied to the series of density profiles from laboratory experiments. As shown in figure 3(*c*), an almost uniform vertical density distribution is observed in the well-mixed state in most cases, and the data of density profiles show that ΔB remains invariant with time over 3 h. The parameters were evaluated as $\alpha = (f_b S_b^{3/2}/f_s S_s^{3/2})$ and $\gamma = H^4 Q/(a_4 f_s S_s^{3/2} M^{1/2})^3$ directly from the experimental condition, where $a_4 = a_2(1+a_3^2/2)^{1/2}$. The measurements of D_0 in terms of γ for the case of no bottom mixing showed a good agreement with the numerical results represented by (4.12), which supports the appropriateness of the evaluation of γ.

Figure 7 shows a criterion for predicting the formation of a thermocline, obtained from the procedure described above. For a given γ, the maximum/minimum values of α were computed with/without the formation of a thermocline, and the results are indicated by horizontal bars; and experimental results are shown by symbols. Generally, good agreement is observed between the two types of data sets.

It shows that as the position of a thermocline approaches the bottom, i.e. $D_0/H \to 1$, the well-mixed state is more likely to occur owing to the bottom mixing. It is expected that when D_0/H becomes larger than 1, the critical value of α becomes 0, because the water column is always in a well-mixed state in this case.

5.4. *The depth of a thermocline*

Careful inspection of figure 4 also reveals an interesting feature which helps in finding the criterion for the formation of a thermocline. When there is no thermocline, the minimum of the density gradient $\partial B/\partial z$ always remains at the surface. On the other

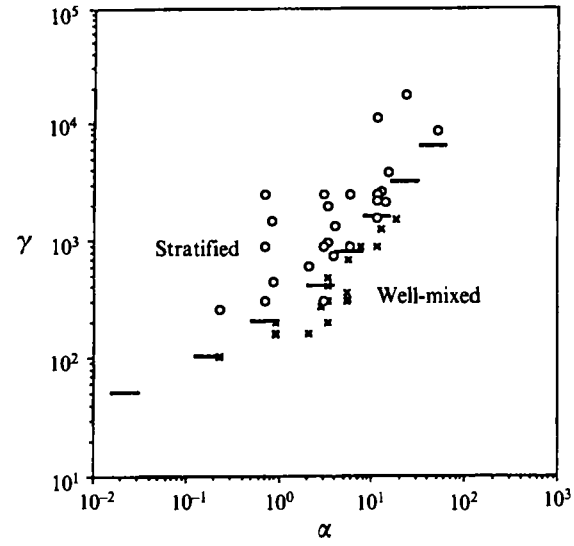

FIGURE 7. The criterion for the formation of a front. For a given γ, the maximum/minimum values of α computed with/without the formation of a thermocline are indicated by horizontal bars. Experimental results are shown by the symbols (○, stratified state; ×, well-mixed state).

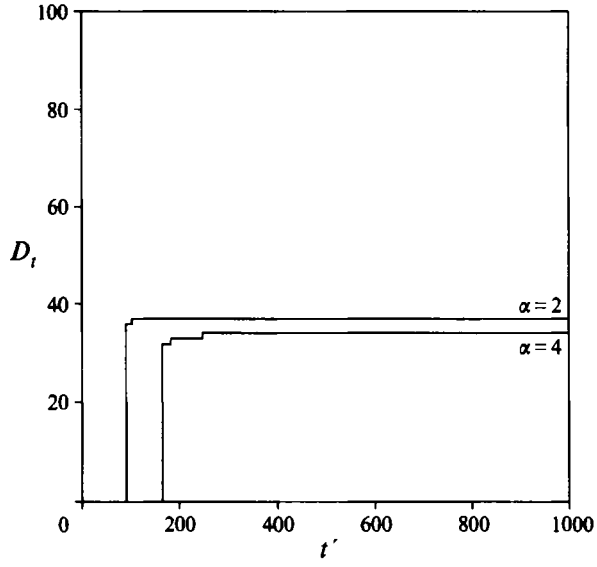

FIGURE 8. The variation of the position of the minimum density gradient with time for $\alpha = 2$ and 4 when $\gamma = 800$.

hand, when a thermocline appears, it jumps to the position of the thermocline. The variation of the depth of the minimum $\partial B/\partial z$ with time is shown in figure 8 for the cases given in figure 4. The equilibrium depth of a thermocline D is obtained from the limiting value of the instantaneous depth D_t as t' goes to infinity. In practice, as shown in figure 8, the calculations clearly show the convergence of D_t to an asymptotic value corresponding to D soon after the appearance of the non-zero D_t. The calculations were performed until $\mathrm{d}D_t/\mathrm{d}t < 10^{-3}$ was satisfied.

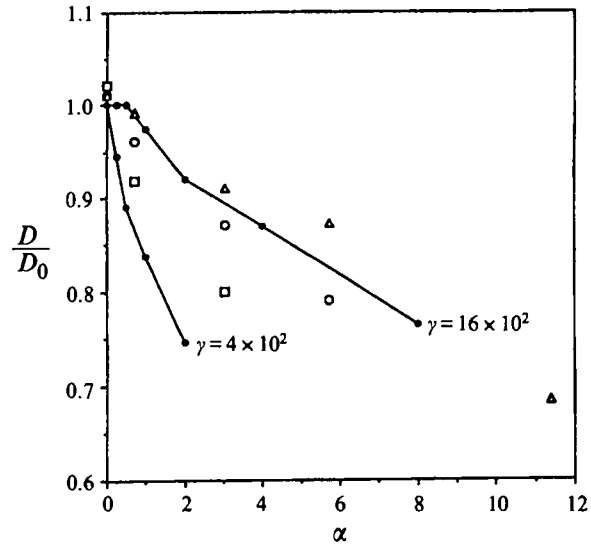

FIGURE 9. The variations of the depth of the thermocline D with α. The lines are the numerical results, and the symbols are the experimental data: □, $\gamma = 297$; ○, $\gamma = 879$; △, $1 = 2000$.

For the determination of the depth of a thermocline in the laboratory experiments the shadowgraph method was used as in previous experiments (Kantha & Long 1980; Hopfinger & Linden 1982; Noh & Long 1990). After the buoyancy flux and grid oscillations were turned off, a few minutes were allowed until the fluctuating motions at the interface died out, and then the measurements were made. The accuracy of the measurements was ± 0.1 cm. These locations of the thermocline were equivalent to the points of intersections between two straight lines in the density profiles: one representing the density of the lower layer and the other representing the mean density gradient in the interfacial layer.

Figure 9 shows the variations of D/D_0 with α for given γ, based on both experimental and numerical data. It is interesting to observe that D decreases with the increase of the bottom mixing for a given γ. When a weak density stratification is developed to form a thermocline, it is exposed to erosion from below by the bottom mixing. This may cause a shift of the position of a thermocline upward. It is also found that when D_0 is large so that the position of a thermocline is closer to the bottom, D becomes more sensitive to α.

6. Interpretation

The result of Hopfinger & Linden (1982), (1.2), suggests that the critical condition for the formation of stratification in the mixed layer can be given by $\beta \sim$ constant. The critical condition from the present investigation, in which the effects of surface mixing are also included, is given by figure 7, and this can be replotted in terms of α and β as shown in figure 10. It is found that the critical values of β, at which the transition occurs, decreases with α, when the flow is affected by the surface mixing. That is, a well-mixed layer is more likely to occur as α becomes larger. The depth at which a thermocline can be formed decreases with decreasing α for a given β. As the distance from the turbulence source at the bottom to the position of thermocline formation increases, the turbulent kinetic energy available there will be smaller, and hence it becomes more difficult to inhibit the formation of a thermocline. The dependence of β

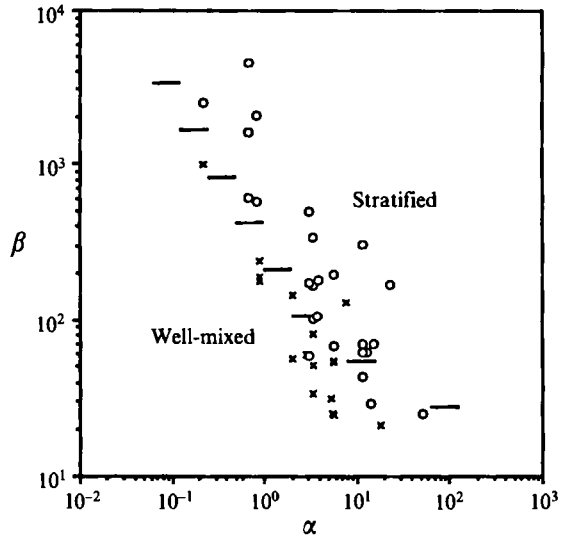

FIGURE 10. The criterion for the formation of a front in terms of α and β (for symbols see figure 7).

on α is found to become weaker, however, as β becomes small ($\beta < 10^2$). This suggests that, if β becomes sufficiently small, the bottom mixing itself becomes strong enough to mix the whole water column regardless of the surface mixing, as was shown in Hopfinger & Linden's (1982) experiment. They also found the critical value of β for the onset of runaway stratification within a thin surface layer to be $\beta \sim 1$–10. It can be inferred from figure 10 that the water column will be always in the mixed state regardless of α as β approaches the critical value.

The importance of surface mixing for the prediction of the formation of stratification was first considered by Fearnhead (1975), who correctly suggested that the work required to maintain the well-mixed state is equal to the potential energy difference ϕ between the well-mixed state and the stratified state with a thermocline at $z = H - D_0$:

$$\phi = BD_0(H - D_0)/2. \tag{6.1}$$

The rate of working required to maintain the mixed state is then given by

$$\frac{\mathrm{d}\phi}{\mathrm{d}t} = \tfrac{1}{2}Q(H - D_0), \tag{6.2}$$

from $Q = \mathrm{d}(BD_0)/\mathrm{d}t$ and $\mathrm{d}D_0/\mathrm{d}t = 0$.

The turbulent kinetic energy flux from the bottom F_b can be calculated from the steady-state solution (3.4) with no stratification ($\partial B/\partial z = 0$) as

$$\frac{\partial F_b}{\partial z} - \epsilon_b = 0, \tag{6.3}$$

where

$$F_b = K_b \frac{\partial E_b}{\partial z}. \tag{6.4}$$

From integration of (6.3), the energy flux is obtained as

$$F_b(z = 0) \sim U_b^3. \tag{6.5}$$

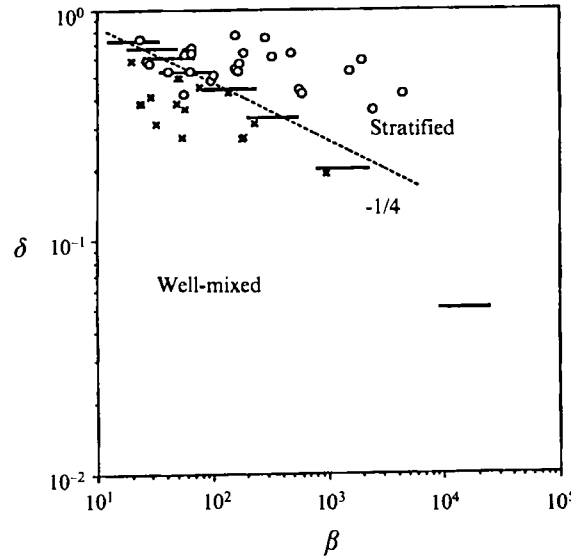

FIGURE 11. The criterion for the formation of a front in terms of β and δ (for symbols see figure 7).

Fearnhead (1975) suggested that the criterion for the formation of a thermocline is determined by the parameter β_δ^* based on the kinetic energy flux near the bottom $F_b(z=0)$, which is expressed as

$$\beta_\delta^* \sim \frac{\mathrm{d}\phi/\mathrm{d}t}{F_b(z=0)} \tag{6.6}$$

$$\sim Q(H-D_0)/U_b^3 \tag{6.7}$$

$$\sim \beta'\delta, \tag{6.8}$$

where $\delta = 1-D_0/H$ and $\beta' = QH/U_b^3 = (H/L)^{-3}\beta$. It is noted that Simpson & Hunter (1974) assumed that $D_0 \ll H$ and $U_t \propto U_b$ in deriving (1.1). Since H was fixed during the calculations, β' is proportional to β, so that $\beta_\delta^* \propto \beta\delta$. Figure 11 shows the replot of figure 10 (or figure 7) in terms of β and δ. It does not follow the prediction given by (6.8), and the critical values of β decreases much faster with δ.

Hopfinger & Linden (1982)'s criterion (1.3) implies that the local r.m.s. turbulent velocity at the prospective depth of the thermocline is more relevant to the formation of stratification. Actually it appears more reasonable to presume that what is important to inhibit the thermocline formation is the turbulent kinetic energy flux near the prospective depth of the thermocline rather than that near the bottom. The parameter is then modified as

$$\beta_\delta \sim \frac{\mathrm{d}\phi/\mathrm{d}t}{F_b(z=H-D_0)} \tag{6.9}$$

$$\sim \frac{Q(H-D_0)}{[K_b/(H-D_0)]^3} \tag{6.10}$$

$$\sim \beta\delta^4, \tag{6.11}$$

using the variation of the r.m.s. turbulent velocity with z (see (2.5)).

A good agreement is generally observed between (6.11) and figure 11. As δ

approaches 0, however, the exponent of δ tends to decreases. This may reflect the fact that near the grid the decay of r.m.s. turbulent velocity is slower than that given by $u \propto z^{-1}$ both in the numerical model and in the experimental data (see (2.5) and (3.40)). It can be also inferred from the dotted line in figure 11 that δ becomes 1 at $\beta \cong 5$, which is equivalent to the critical value of β suggested by Hopfinger & Linden (1982).

In the real ocean, however, the wind stress and heat flux on the sea surface may be regarded as constants for a limited geographical area and for a given time period (Simpson *et al.* 1978). Under these conditions (6.11) shows that β is the governing parameter that determines the formation of stratification, which agrees with the previous studies (Simpson *et al.* 1978; Pingree & Griffiths 1978). It is also important to note that (6.11) depends on the decay law of (2.4)–(2.6). If the velocity and length scales of turbulence are given by $E^{1/2} \sim u^*$ and $l \sim z$ as in the boundary layer of turbulent shear flows (Monin & Yaglom 1965), where u^* is the friction velocity, the result (6.8) is obtained instead of (6.11).

7. Summary

In the previous sections, the formation of a thermocline in a water column, in which shear-free turbulence is generated both at the surface and bottom and a stabilizing buoyancy flux is imposed on the surface was described with an aim of understanding the formation of a tidal front. Both laboratory experiments and a numerical model were used in this study.

Depending on the conditions, the water column can develop a two-layered stratified state with a thermocline, or maintain a vertically mixed state with relatively uniform density. The relevant parameters of this case are the buoyancy flux at the surface Q, the eddy diffusivities maintained at the bottom K_{0b} and at the surface K_{0s} and the height of the water column H. In general the criterion for the formation of a thermocline is given by $\beta_0 \delta^4 \sim$ constant, but the exponent of δ in this criterion tends to decrease as δ approaches 0; here $\beta_0 = H^4 Q / K_{0b}^3$, $\delta = 1 - D_0/H$ and D_0 is the depth of a thermocline in the absence of bottom mixing. This criterion can be explained based on the fact that a potential energy increase is required to maintain the mixed state against the stratification induced by buoyancy flux, and this must be supplemented by turbulent kinetic energy flux from the bottom. The result suggests that the formation of a thermocline is determined by the balance between the required potential energy increase of the whole water column and the TKE flux from the bottom to the depth where the thermocline is supposed to form. The depth of a thermocline, when it is formed, decreases with the increase of the bottom mixing for a given value of D_0. This is caused by the erosion of the upper mixed layer by the turbulence propagating from below during the formation of a thermocline.

The laboratory experiments were carried out in the Environmental Fluid Dynamics Laboratory at Arizona State University. During the preparation of this paper, the authors were supported by the Korea Science & Engineering Foundation, the Ministry of Education of Korea and the Physical Oceanography Program of the Office of Naval Research, USA.

REFERENCES

ANDRE, J. C., DE MOOR, G., LACARRERE, P., THERRY, G. & VACHAT, R. DU 1978 Modeling the 24 hour evolution of the mean and turbulent structures of the planetary boundary layer. *J. Atmos. Sci.* **35**, 1861.

BATCHELOR, G. K. 1967 *An Introduction to Fluid Dynamics*. Cambridge University Press.

BRITTER, R. E., HUNT, J. C. R., MARSH, G. L. & SNYDER, W. H. 1983 The effects of stable stratification on turbulent diffusion and the decay of grid turbulence. *J. Fluid Mech.* **127**, 27.

BYE, J. A. T. 1990 Richardson number profiles in laboratory experiments applied to shallow seas. *Geophys. Astrophys. Fluid Dyn.* **51**, 135.

CSANADY, G. T. 1964 Turbulent diffusion in a stratified fluid. *J. Atmos. Sci.* **21**, 439.

FEARNHEAD, P. G. 1975 On the formation of fronts by tidal mixing around the British Isles. *Deep-Sea Res.* **22**, 331.

GALPERIN, G., ROSATI, A., KANTHA, L. H. & MELLOR, G. L. 1989 Modeling rotating stratified turbulent flows with application to oceanic mixed layers. *J. Phys. Oceanogr.* **19**, 901.

HANNOUN, I. A., FERNANDO, H. J. S. & LIST, E. J. 1988 Turbulence near a sharp density interface. *J. Fluid Mech.* **189**, 189.

HOPFINGER, E. J. & LINDEN P. F. 1982 Formation of thermoclines in zero-mean-shear turbulence. *J. Fluid Mech.* **114**, 157.

HOPFINGER, E. J. & TOLY, J. A. 1976 Spatially decaying turbulence and its relation to mixing across density interface. *J. Fluid Mech.* **78**, 155.

KANTHA, L. H. & LONG, R. R. 1980 Turbulent mixing with stabilizing surface buoyancy flux. *Phys. Fluids* **23**, 2142.

MONIN, A. S. & YAGLOM, A. M. 1965 *Statistical Fluid Dynamics*, Vol. 1. MIT Press.

NOH, Y. 1993 A numerical model for the onset of stratification in shear-free turbulence. *Geophys. Astrophys. Fluid Dyn.* **72**, 35.

NOH, Y. & FERNANDO, H. J. S. 1991 A numerical study on the formation of a thermocline in shear-free turbulence. *Phys. Fluids* A **3**, 422.

NOH, Y. & FERNANDO, H. J. S. 1993 The role of molecular diffusion in the deepening of the mixed layer. *Dyn. Atmos. Oceans* **17**, 187.

NOH, Y. & LONG, R. R. 1990 Turbulent mixing in a rotating, stratified fluid. *Geophys. Astrophys. Fluid Dyn.* **53**, 125.

PEARSON, H. J., PUTTOCK, J. S. & HUNT, J. C. R. 1983 A statistical model of fluid-element motions and vertical diffusion in a homogeneous stratified turbulent flow. *J. Fluid Mech.* **129**, 219.

PINGREE, R. D. & GRIFFITHS, D. K. 1978 Tidal fronts on the shelf seas around the British Isles. *J. Geophys. Res.* **83**, 4615.

SIMPSON, J. H., ALLEN, C. M. & MORRIS, N. C. G. 1978 Fronts on the continental shelf. *J. Geophys. Res.* **83**, 4607.

SIMPSON, J. H. & HUNTER, J. H. 1974 Fronts in the Irish Sea. *Nature* **250**, 404.

SRDIC, R., FERNANDO, J. H. S. & MONTENEGRO, L. 1995 Generation of nearly isotropic turbulence using two oscillating grids. *Exps. Fluids* (in press).

TURNER, J. S. 1986 Turbulent entrainment: the development of the entrainment assumption, and its application to geophysical flows. *J. Fluid Mech.* **173**, 431.